Biophysical *Journal*
Article

Biophysical Society

Mobility of Lower MA-Helices for Ion Conduction through Lateral Portals in 5-HT_{3A} Receptors

Antonia G. Stuebler[1] and Michaela Jansen[1,*]
[1]Department of Cell Physiology and Molecular Biophysics and Center for Membrane Protein Research, School of Medicine, Texas Tech University Health Sciences Center, Lubbock, Texas

ABSTRACT The intracellular domain of the serotonin type 3A receptor, a pentameric ligand-gated ion channel, is crucial for regulating conductance. Ion permeation through the extracellular vestibule and the transmembrane channel is well understood, whereas the specific ion conduction pathway through the intracellular domain is less clear. The intracellular domain starts with a short loop after the third transmembrane segment, followed by a short α-helical segment, a large unstructured loop, and finally, the membrane-associated MA-helix that continues into the last transmembrane segment. The MA-helices from all five subunits form the extension of the transmembrane ion channel and shape what has been described as a "closed vestibule," with their lateral portals obstructed by loops and their cytosolic ends forming a tight hydrophobic constriction. The question remains whether the lateral portals or cytosolic constriction conduct ions upon channel opening. In our study, we used disulfide bond formation between pairs of engineered cysteines to probe the proximity and mobility of segments of the MA-helices most distal to the membrane bilayer. Our results indicate that the proximity and orientation for cysteine pairs at I409C/R410C, in close proximity to the lateral windows, and L402C/L403C, at the cytosolic ends of the MA-helices, are conducive for disulfide bond formation. Although conformational changes associated with gating promote cross-linking for I409C/R410C, which in turn decreases channel currents, cross-linking of L402C/L403C is functionally silent in macroscopic currents. These results support the hypothesis that concerted conformational changes open the lateral portals for ion conduction, rendering ion conduction through the vertical portal unlikely.

SIGNIFICANCE The intracellular domain (ICD) of pentameric ligand-gated ion channels (pLGICs) is the most diverse domain within receptors of the Cys-loop superfamily. Despite being the least understood domain of pLGICs, its impact on ion-channel function and contribution to the cytosolic exit pathway of the channel have not been investigated. X-ray and cryo-EM structures have captured the structured segments of the ICD of 5-HT_{3A} receptors in different conformational states with lower resolution of the ICD as compared with the other domains. Here, we provide experimentally derived evidence for the importance of the differential mobility of the cytosolic segment of the MA-helices, which supports the existence of lateral portals as opposed to a vertical pathway for 5-HT_{3A} receptors.

INTRODUCTION

5-hydroxytryptamine 3 receptors (5-HT_3Rs) are pentameric ligand-gated ion channels (pLGICs) in the family of Cys-loop receptors, which also include the cationic nicotinic acetylcholine (nAChR) and the anionic γ-aminobutyric acid ($GABA_A$R) and glycine receptors (GlyR). This superfamily is responsible for fast neuronal excitatory and inhibitory neurotransmission in the central nervous system by conducting selected ions across the membrane upon neurotransmitter binding (1,2). The overall structure of pLGICs is conserved. Each subunit consists of three separate domains: the extracellular (ECD), transmembrane (TMD, M1–M4), and intracellular domains (ICD). The ICD of eukaryotic pLGICs, primarily between transmembrane segments M3 and M4, is the most diverse domain with regard to length (50–280 amino acids) and amino acid composition across the family (3).

Successively, structural studies of 5-HT_{3A}R (4–7) and nAChR (8–11) determined that the ICD consists of the following structural elements: a short post-M3 loop (L1), an amphipathic MX-helix, a long loop (L2) of 60 unresolved amino acids, and the membrane-associated helix (MA-helix), which is continuous with the M4-transmembrane segment (12).

Submitted August 24, 2020, and accepted for publication October 27, 2020.
*Correspondence: michaela.jansen@ttuhsc.edu
Editor: Sudha Chakrapani.
https://doi.org/10.1016/j.bpj.2020.10.029

The ICD influences different aspects of receptor function. The ICD of cation-conducting pLGICs is the site for differential modulation of functional surface expression by chaperone proteins. The chaperone resistance to inhibitors of choline esterase (RIC-3) was shown to be necessary for assembly and trafficking of DEG-3 acetylcholine receptors in *Caenorhabditis elegans*. Subsequent studies found that RIC-3 modulates functional expression of nAChR $\alpha7$, $\alpha3\beta4$, and $\alpha4\beta2$, as well as 5-HT_{3A}R (13–17). For the 5-HT_{3A}R-RIC-3 interaction, we found that the ICD is required and sufficient for the interaction (18–22) and, more recently, that a 24-amino acid peptide of the 5-HT_{3A}-subunit ICD interacts with RIC-3 (23). The ICD, in particular the MA-helix of 5-HT_{3A}R, was shown to control Ca^{2+} permeability and ion permeation (24), and deletions within the ICD abolished inward rectification (3). Overall, this indicates that the ICD has very rich and widespread functional implications.

Studies have also demonstrated that the ICD can limit the receptor's single-channel conductance (γ) (25) because it contains the portal(s) for ion access to the cytosol. The first structures of the ICD of *Torpedo marmorata* depicted five narrow openings between adjacent MA-helices, triggering predictions for lateral portals at the TMD-ICD interface (12,26). Structure-function studies based on homology models have since investigated this stretch within the MA-helices and identified specific residues that can influence the receptor's single-channel conductance (25,27–30). Specifically, three conserved arginines in the 5-HT_{3A} subunit increase the conductance of the receptor ~33-fold when mutated to their human 5-HT_{3B} subunit counterparts (R432Q/R436D/R440A) (25). Using mutagenesis and Cys scanning and modifications, it was concluded that ions conduct through lateral portals for the triple 5-HT_{3A}-QDA-mutant receptor and that the 5-HT_{3A}-wild-type receptor has a low single-channel conductance because of steric hindrance and static repulsion by its positively charged residues in the MA-helices (27–29). In reciprocal experiments with $\alpha4\beta2$ nAChRs, the introduction of arginines at aligned positions reduced the conductance (29). However, the conductance was not fully limited to the characteristically low single-channel conductance of the 5-HT_{3A} homomeric receptor, raising the question of whether other factors are involved in the 5-HT_{3A}R's 0.6 pS conductance.

More recently, with additional high-resolution structural data becoming available, two alternate exit pathways for ions through the 5-HT_{3A}R became apparent: one through the five lateral portals and another through a vertical portal in continuation with the pore of the transmembrane channel (Fig. S1 *C*; (4,6)). Although the vertical portal is equipped with a much larger pore diameter (4.2 Å) in the crystal structure, the inside of the pore is lined with hydrophobic residues, plugging the cytosolic end (6,8). In closed-pore conformation(s), on the other hand, the lateral portals are obstructed by positively charged residues and the L1-loop threading through them (5,6). Clearly, to elucidate the ion pathway through the channel, conformational changes of the ICD have to be investigated further.

The overall movement of the receptor entails a global twisting of the ECD and TMD around the central pore (counterclockwise and clockwise for ECD and TMD, respectively), similar to other pLGICs (31,32). Much of this information was first described for the prokaryotic homologs from *Gloeobacter violaceus* and *Erwinia chrysanthemi* (33–35). These receptors could be captured in the open and closed states but lack the ICD only found in eukaryotic pLGICs. The exact conformational changes of the ICD remain largely unexplored, but it is known that the ICD undergoes agonist-mediated structural changes and that the MA stretch may be a mobile structure (36). The flexibility of the MA-helices was even shown to be a determining factor in controlling single-channel conductance in 5-HT_{3A}Rs (37).

A recent cryo-electron microscopy (cryo-EM) structure captured the 5-HT_{3A}-ICD in its presumably open state with the lateral portals in a conformation conducive for ion translocation (4). In this structure, the TMD-ICD interface cavity is enlarged by a helical break within the upper section of the MA-helix, and the MX-helix is moved outward and upward toward the membrane (Fig. S1 *B*).

Previously, we have shown that the 5-HT_{3A}-ICD alone assembles into pentamers (18) and that disruption of salt bridges in conjunction with the QDA substitution also abolishes assembly of the 5-HT_{3A}-ICD into pentamers (38). In this study, we investigated the mobility of the lower end of the MA-helices (L402-R410, Fig. 1), a segment of the MA stretch that remains largely unexplored. This segment starts two α-helical turns below the lowest of the three arginines, $-4'$ or R416 (mouse 5-HT_{3A}R, equivalent to R432 in the human sequence), and extends for about two more helical turns (Fig. 1). We engineered cysteine pairs three and five helical turns below the lateral portals and used disulfide trapping to probe the movement at two different levels of the 5-HT_{3A}-ICD. Through our experiments, we demonstrate that mobility of the MA-helices just below the lateral portals is required to open the cytosolic ion access pathway. On the contrary, inhibiting mobility at the very bottom of the MA-helices, in closer proximity to the vertical opening, had no functional effect on ion conduction at the macroscopic level.

MATERIALS AND METHODS

Materials

Copper(II) sulfate pentahydrate (Sigma-Aldrich, St. Louis, MO), 1,10-phenanthroline (Sigma-Aldrich), NEM (*N*-ethylmaleimide; Sigma-Aldrich), DTT (dithiothreitol; Thermo Fisher Scientific, Fair Lawn, NJ), EGTA (ethyleneglycol-bis(β-aminoethyl)-N,N,N′,N′-tetraacetic acid tetrasodium $\geq$97%; Sigma-Aldrich), and 5-HT (serotonin hydrochloride; Sigma-Aldrich) were used. Stock of serotonin (2 mM), copper(II) sulfate (100 mM), and DTT (1 M) were prepared in distilled water. 1,10-Phenanthroline (0.5 M) was dissolved in dimethyl sulfoxide. All solutions,

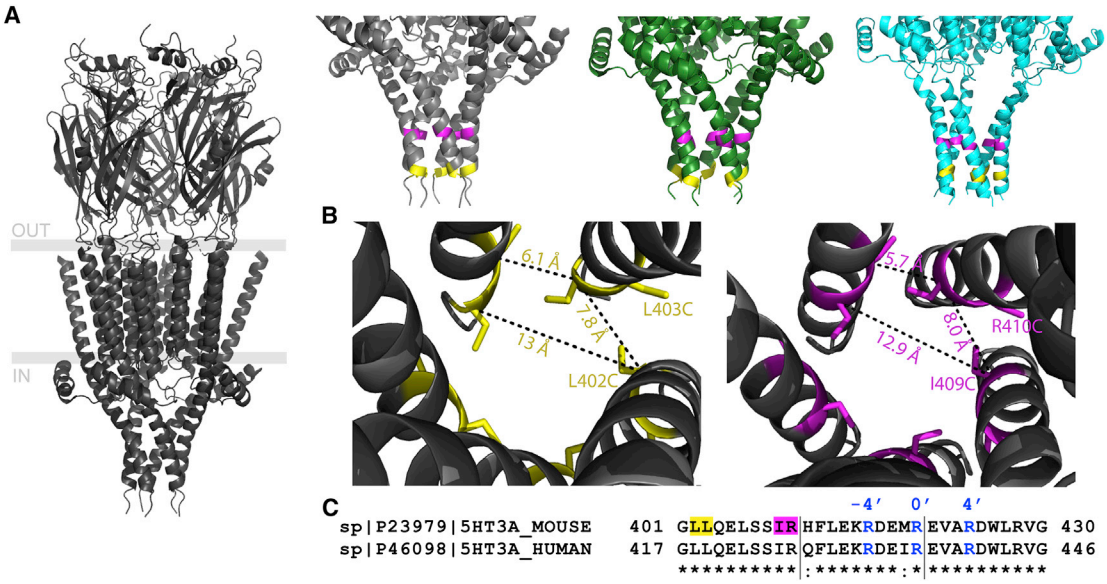

FIGURE 1 Distances between cysteine pairs engineered in MA-helices in 5-HT_{3A}Rs measured between adjacent and nonadjacent subunits. (*A*) Left: ribbon diagram of the structure of the full length 5-HT_{3A}R (PDB: 4PIR) with membrane boundaries indicated by gray lines viewed parallel to the membrane. Right: zoomed-in view of the 5-HT_{3A}-ICD in different functional conformations. PDB: 4PIR is shown in the presence of an inhibiting antibody, non-conducting state (*gray*); PDB: 6HIO is shown in the presence of 5-HT, intermediate state (*green*); PDB: 6DG8 is shown in the presence of 5-HT, conducting state (*cyan*) viewed parallel to the membrane. Yellow (L402/L403) and magenta (I409/R410) residues denote positions where Cys pairs were introduced. (*B*) Cartoon representations of the ICD of 5-HT_{3A}R (PDB: 4PIR), viewed perpendicular to the membrane down the pore, are given, showing L402C-L403C (*yellow*, *left*) and I409C-R410C (*magenta*, *right*) residues and the distances between their α-carbons. (*C*) Sequence alignment of the MA-helices of mouse and human 5-HT_{3A}Rs is shown with the three arginines mutated to QDA indicated in blue (R−4′, R0′, R4) and the residues mutated to Cys highlighted in yellow (L402-L403) and magenta (I409-R410), respectively.

including the Cu:Phe solution, were made in oocyte ringer buffer (OR-2) immediately before experiments were conducted.

Molecular biology

Cysteines were engineered into the mouse 5-HT_{3A}R (GeneBank: AAT37716) in the pGEMHE vector for oocyte expression (39), which contains a V5-tag (GKPIPNPLLGLDSTQ) close to the N-terminus (22). The desired basepairs coding for Cys were introduced using overlapping primers with the QuikChange II site-directed mutagenesis kit (Agilent Technologies, Santa Clara, CA) and were confirmed by DNA sequencing (GENEWIZ, South Plainfield, NJ). The amino acid sequence numbering used corresponds to the numbering of the mature sequence as published with the X-ray structure (6). There are three endogenous cysteines in the ICD of 5-HT_{3A} subunits, two in the L2-loop and one ~40 Å apart from the engineered cysteine residues in the X-ray structure (6). cDNA was linearized with the *Nhe*I restriction enzyme and in vitro transcribed with the T7 RNA polymerase kit (mMESSAGE mMACHINE T7 Kit; Applied Biosystems/Ambion, Austin, TX). Complementary RNA (cRNA) was purified with the MEGAclear Kit (Applied Biosystems/Ambion) and precipitated using 5 M ammonium acetate. The cRNA was subsequently dissolved in nuclease-free water and stored at −80°C.

Xenopus laevis oocyte preparation and injection

X. laevis oocytes were isolated, enzymatically defolliculated, and stored as previously described (40). *X. laevis* were handled and maintained following procedures approved by the local animal welfare committee (Institutional Animal Care and Use Committee, IACUC #08014, PHS Assurance #A 3056-01). Before injection, oocytes were washed in OR-2 (115 mM NaCl, 2.5 mM KCl, 1.8 mM MgCl2, 10 mM HEPES (pH 7.5)) and maintained in standard oocyte saline medium (100 mM NaCl, 2 mM KCl, 1 mM $MgCl_2$, 1.8 mM $CaCl_2$, 5 mM HEPES (pH 7.5) supplemented with 1% antibiotic-antimycotic (100X, 10,000 units/mL of penicillin, 10,000 mg/mL of streptomycin, and 25 mg/mL amphotericin B; Gibco, Thermo Fisher Scientific, 5% horse serum) for up to 7 days at 16°C. Oocytes were microinjected with 10 ng of in vitro synthesized complementary RNA (cRNA) (200 ng/μL) using an automatic oocyte injector (Nanoject II; Drummond Scientific, Broomall, PA). Depending on the construct injected, sufficient expression could be seen 24–48 h after injection.

Electrophysiology

Two-electrode voltage-clamp recordings were conducted 1–3 days after injection. The currents were recorded and amplified using a TEV-200A amplifier (Dagan Instruments, Minneapolis, MN), a Digidata 1440A data interface (Molecular Devices, Sunnyvale, CA), and a MiniDigi 1B (Molecular Devices), all controlled by pClamp 10.7 software (Molecular Devices). The oocytes were perfused with OR-2 using gravity flow at an approximate rate of 5 mL/min in a 250 μL chamber. The reagents (Cu:Phe, DTT, and EGTA) were dissolved in OR-2 and perfused in the same manner. All experiments were performed at room temperature (RT, 22–24°C) and a holding potential of −60 mV. The glass pipettes were filled with 3 M KCl and had a resistance of below 2 MΩ. Currents were evoked by 3 μM 5-HT unless otherwise stated, and the agonist was applied until a stable response was observed to record a maximal current response. The EC_{50} for 5-HT_{3A}-QDA-I409C/R410C was determined in the presence of 10 mM DTT to minimize disulfide bond formation.

Oocyte protein isolation

X. laevis oocytes expressing 5-HT_{3A}-wild-type (wt) and 5-HT_{3A}-Cys constructs were incubated either in 100:200 μM Cu:Phe or 3 μM 5-HT for 2

min before being homogenized. Uninjected oocytes were treated similarly as control. A crude membrane protein fraction was isolated as described before (41). In brief, oocytes were homogenized using a 200 μL pipette tip in ice-cold vesicle dialysis buffer (VDB; 100 μL/oocyte: 96 mM NaCl, 0.1 mM EDTA, 10 mM MOPS, 0.02% NaN_3, 2 mM NEM (pH 7.5)), supplemented with protease inhibitor cocktail III (PI, 2 μL/mL; Research Products International, Mt. Prospect, IL), and centrifuged (800 $\times$ g for 10 min at 4°C). The supernatant was collected, and proteins were obtained by high-speed centrifugation (39,000 $\times$ g for 1 h at 4°C). The crude membrane pellet was resuspended in VDB without NEM (3 μL/oocyte), supplemented with PI cocktail, and stored at −80°C.

Western blotting

For SDS-electrophoresis, proteins isolated as crude membranes as described above, were separated using 4–15% precast gradient TGX Stain-Free gels (Bio-Rad, Hercules, CA) for 35 min at 200 V. Proteins were transferred to polyvinylidene difluoride membranes using the Trans-Blot Turbo Transfer System (Bio-Rad). Membranes were blocked with 5% blotting-grade blocker (Bio-Rad) in Tween-Tris-buffered saline (TTBS, 100 mM Tris (pH 7.5), 0.9% NaCl, 1% Tween-20 [25–30 mL/membrane]) overnight. The membranes were incubated with the primary V5 horseradish peroxidase (HRP)-conjugated antibody (1:5000, V5-HRP antibody; Invitrogen, Carlsbad, CA) in TTBS with 5% blotting-grade blocker overnight at 4°C. After the removal of the primary antibody, the membranes were washed five times for 5 min with TTBS. Proteins were visualized by chemiluminescent detection (ImageQuant LAS 4000; GE Healthcare Life Sciences, Chicago, IL) of peroxidase substrate activity (SuperSignal West Femto Maximum Sensitivity Substrate; Thermo Fisher Scientific). Band intensities were quantified using UN-SCAN-IT gel (Silk Scientific, Orem, UT). The DTT-resistant band (running at ~130 kDa) was excluded from the quantification but caused the background of the membrane to appear darker in close proximity to the location of the dimer, potentially increasing the band intensity.

Data analysis

Data were analyzed using pClamp, Origin (OriginLab, Northampton, MA), Prism 6 Software (GraphPad Prism, La Jolla, CA), and UN-SCAN-IT gel (Silk Scientific). Data are shown as mean ± standard deviation (SD) ($n \geq 3$), with the maximal current induced by 5-HT as the normalizing standard (100% of current response) for other current amplitudes recorded in the same oocytes. Statistical significance was determined with unpaired t-test, paired t-test between the initial inward current and each set of conditions, or one-way ANOVA, Dunnett's multiple comparisons test ($^*p \leq 0.01$ unless otherwise stated). All figures and graphs were made in Origin, PyMOL Molecular Graphics System (Schrödinger), and Adobe Illustrator CC 2018.

RESULTS

Design of engineered cysteine pairs, L402C-L403C and I409C-R410C, to cross-link MA-helices in 5-HT_{3A}Rs

To investigate the mobility of the cytosolic end of the intracellular domain of 5-HT_3ARs, we engineered two different cysteine pairs below the proposed lateral portals at different levels in the ICD, almost two helical turns apart: L402C-L403C (Fig. 1, *yellow*) and I409C-R410C (Fig. 1, *magenta*). For each double-Cys construct, the mutated cysteines are adjacent to one another on the same subunit (Fig. 1 *B*), with side chains extending toward the cysteines on adjacent subunits. Given that the average Cα-Cα' carbon distance for the engineered Cys in adjacent subunits is similar to the average distance found between disulfide-bonded cysteines of 5.6 Å (42,43), cysteines placed at these locations should enable cross-linking of MA-helices (Table 1). Both the orientation of the side chains and α-carbon separation predispose the L402C-L403C and I409C-R410C Cys pairs for disulfide bond formation. All other side chain orientations or distances in between these positions, specifically MA-helix positions 404 through 408, are less suited for disulfide bond formation, with the next closest distance of 6.4 Å between E404 and L406. Double-cysteine pairs were introduced in the full length 5-HT_{3A}-wt and 5-HT_{3A}-QDA background containing the triple substitution QDA to compare the impact of MA-flexibility in low- (5-HT_{3A}-wt) and high- (5-HT_{3A}-QDA) conductance receptors.

L402C-L403C and I409C-R410C Cys pairs form intersubunit disulfide bonds as visualized in Western blots after SDS-PAGE separation

To evaluate whether each Cys pair promotes intersubunit cross-linking (i.e., disulfide bridge formation between MA-helices), we compared the oligomeric state/s induced by oxidizing and reducing conditions, as well as by application of the agonist, of each Cys construct to the background receptor (5-HT_{3A}-wt or 5-HT_{3A}-QDA) by Western blot after SDS-polyacrylamide gel electrophoresis (PAGE) (Fig. 2). Constructs were expressed in *X. laevis* oocytes and were then exposed to an oxidizing agent for 2 min to promote an oxidizing environment for disulfide bond formation. 1,10-Phenanthroline in the presence of copper ions (Cu:Phe, 100:200 μM) is an oxidizing agent that has been widely used as a catalyst for oxidation of sulfhydryl groups to disulfides (44–47). Its oxidative mechanism involves diffusible reactive intermediates that can penetrate membranes and protein interiors (48–50). The Cu:Phe treatment was followed by a wash, and then the oocytes were homogenized to generate crude membrane protein fractions. In a separate

TABLE 1 . Distances in Å between α-Carbons of Engineered Cysteines and Pore Diameters in Different X-Ray and Cryo-EM Structures, as Measured in Pymol

	L402C-L403C			I409C-R409C		
	Across the Pore	Adjacent Subunit		Across the Pore	Adjacent Subunit	
PDB	L402C-L403C	L402C-L403C	L402C-L402C	I409C-R410C	I409C-R410C	I409C-I409C
4PIR (X-ray)	13.0	6.1	7.8	12.9	5.7	8.0
6BE1 (apo, closed)	14.7	7.3	9.4	13.6	7.4	9.1
6DG8 (state 2 open)	15.4	7.7	9.0	15.3	8.3	9.5
6HIN (F active state)			ICD Unresolved			
6HIO (I1 intermediate)	14.8	6.9	8.8	13.9	6.6	7.7

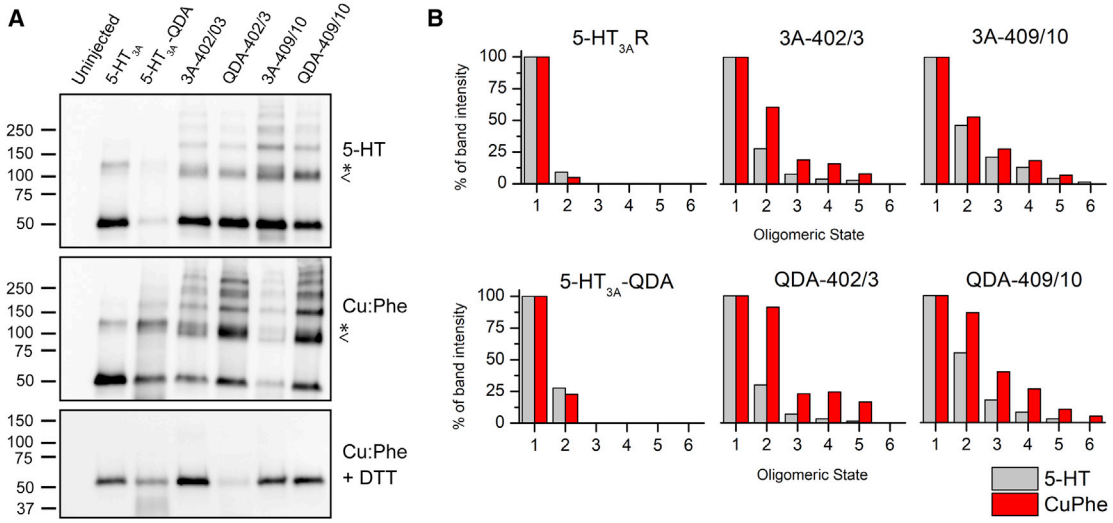

FIGURE 2 Agonist or Cu:Phe application induce disulfide bond formation for L402C-L403C and I409C-R410C expressed in *Xenopus* oocytes. (*A*) Receptor-expressing *X. laevis* oocytes were treated to mimic the electrophysiological experiments (either exposed to 2 min of 3 μM 5-HT or 100:200 μM Cu:Phe). Crude membrane fractions were separated by SDS-PAGE in the absence of reducing agent (*top panel*: oocytes treated with 5-HT, *middle*: with Cu:Phe), and loading was adjusted for construct-dependent expression levels. A monomer band (55 kDa) is observed for all constructs and higher cross-linked oligomeric states for all double-Cys mutants. Note that a band (indicated by *) running at a slightly higher molecular weight than dimers (indicated by <) is seen in all samples (~130 kDa), including in the absence of engineered Cys. Oxidized membrane fractions were also separated in sample buffer with reducing agent (DTT) to show release of the cross-link through disulfide reduction (*bottom panel*). (*B*) The band intensity was quantified using UN-SCAN-IT gel. Monomer bands were used as control (100%) for each construct with each condition. The background band at a slightly higher molecular weight than dimer present in all samples leads to some "dimer" signal in the wt 5-HT_{3A}R and QDA-R. Overall, Cu:Phe (*red bars*) increases the prevalence of cross-linked species compared to agonist (*gray bars*), which appears to be more pronounced in the QDA-R background.

second group, oocytes expressing 5-HT_{3A}-wt and individual constructs were exposed to the agonist (3 μM 5-HT) for 2 min instead to compare the effect of agonist-induced versus oxidizing-agent-induced cross-linking. Each condition used 16 or more oocytes. 5-HT_{3A}-subunits were detected via a V5-epitope tag located near the N-terminus (Fig. 2 *A*). The band intensities varied with different expression levels and were adjusted accordingly for each lane. For all 5-HT_{3A} constructs (wild-type and substitution constructs), a monomer band at ~55 kDa (Fig. 2 *A*) is observed, which is equivalent to the theoretical molecular weight of the monomer. There is also a second band present in all lanes (band indicated by *) that has previously been observed upon extraction of the channel from oocytes and runs at a slightly higher molecular weight (~130 kDa) than the expected dimer (~110 kDa, indicated by <).

Larger bands (>150 kDa) are visible for each L402C-L403C and I409C-R410C Cys pair, indicating that subunits containing these substitutions form higher oligomeric states in the presence of 5-HT or Cu:Phe (Fig. 2 *A*). The presence of these higher-molecular-weight bands was completely reversed by reduction of the Cu:Phe crude membrane fractions with DTT under denaturing conditions, suggesting that they represent oligomers stabilized by disulfide bridges (Fig. 2 *A*, *bottom panel*). Additionally, the different band intensities were quantified using UN-SCAN-IT gel and are shown as percentages normalized to the monomer band set to 100% for each oligomeric state and each construct (Fig. 2 *B*). Although the dimer band is prominently present in all Cys pairs, higher oligomeric bands have a larger intensity in the 5-HT_{3A}-QDA background of the Cys pairs as compared with the regular 5-HT_{3A}-wt background (Fig. 2 *B*).

Agonist-induced current reduction observed in macroscopic currents

To test functionality of double-Cys receptors and the stability of their current responses, we measured 5-HT-induced currents from *X. laevis* oocytes expressing 5-HT_{3A}-wt, 5-HT_{3A}-QDA, and their respective Cys-pair substitution constructs using two-electrode voltage-clamp recordings (Fig. 3 *A*). All receptors exhibited inward currents in response to the application of 3 μM 5-HT, a concentration ~5-fold above EC_{50}-values for 5-HT_{3A}-wt, 5-HT_{3A}-QDA, and 5-HT_{3A}-QDA-I409C/R410C (22), indicating that double-Cys channels form functional receptors. Brief and repeated 5-HT exposures demonstrated that the inward current amplitudes of 5-HT_{3A}-wt, 5-HT_{3A}-QDA, and double-Cys pair L402C-L403C constructs in either background were stable (variations <10%; Fig. 3 *A*).

In contrast to the other receptors, the Cys pair I409C-R410C in both backgrounds showed current attenuation with repeated 5-HT application (Fig. 3 *A*, *bottom traces*) until a stable level was reached, ~38 and ~27% of the original current, for 5-HT_{3A}-I409C/R410C and 5-HT_{3A}-QDA-I409C/R410C, respectively. This decrease in current was

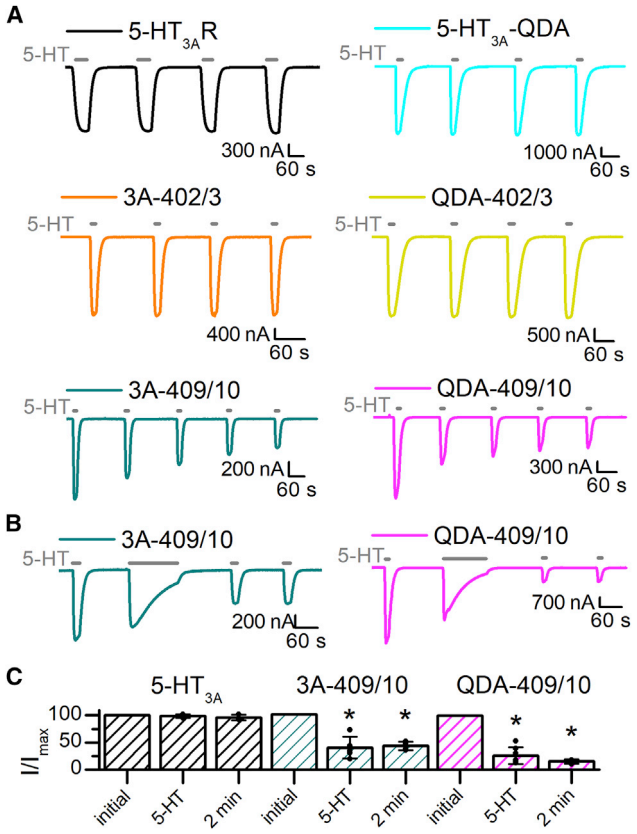

FIGURE 3 Agonist-induced current reduction of the double-Cys pair I409C-R410C induced by agonist application(s). (*A*) Sample traces of currents recorded from *X. laevis* oocytes expressing wt 5-HT_{3A}Rs and engineered constructs in response to 3 μM 5-HT are shown (*gray bars*). For test currents, 5-HT was applied until a maximal current amplitude was reached, 15–60 s. 5-HT_{3A}Rs (*black*), QDA-Rs (*teal*), 5-HT_{3A}-L402C/L403C (*orange*), and QDA-L402C/L403C (*yellow*) show stable responses to repeated applications of the agonist, with both the current amplitudes and kinetics unaltered. 5-HT_{3A}-I409C/R410C (*green*) and QDA-I409C/R410C (*magenta*) show successively decreasing current amplitudes with each 5-HT-application until a stable response is reached. (*B*) Sample traces of 5-HT_{3A}-I409C/R410C (*green*) and QDA-I409C/R410C (*magenta*) in response to 3 μM 5-HT are shown (*gray bars*). The initial inward current represents the reference current amplitude (100% of current) and is followed by an agonist application of 2 min. After this prolonged 5-HT exposure, both Cys pairs exhibit reduced but stable inward currents. (*C*) Quantification of the reduced current amplitudes after repeated (5-HT) and prolonged (2 min) 5-HT application(s) is also shown in bar graphs. Data are shown as mean $\pm$ SD. Individual data points are shown as circles overlaid on top of the bar graph ($n \geq 3$). Statistical significance was determined with paired *t*-test between the initial inward current and the stable, reduced current amplitude after agonist exposure(s) (*$p \leq 0.01$).

not only induced by repeated agonist application. I409C-R410C receptors also showed profound current attenuation of test currents after a single longer 5-HT exposure of 2 min (Fig. 3 *B*). The current reduction after repeated agonist application was not significantly different than the current attenuation with a longer single 5-HT exposure (unpaired *t*-test, $p > 0.05$). The same experimental setup yielded desensitization of the majority of 5-HT_{3A}Rs during the 2-min agonist application, but no reduction in test current amplitudes of subsequent 5-HT applications (Fig. 3 *C*, *black bars*).

For channels with only a single engineered Cys, 5-HT_{3A}-I409C and 5-HT_{3A}-QDA-I409C, inward current attenuation was not observed (Fig. S2). On the contrary, these channels showed stable responses to agonist application, comparable with 5-HT_{3A}-wt and 5-HT_{3A}-QDA-Rs without engineered Cys.

Effects of Cu:Phe, DTT, and EGTA on 5-HT-induced currents

Oocytes expressing constructs were treated with the oxidizing agent Cu:Phe (100:200 μM) for 2 min (Fig. 4 *A*; Fig. S3 *A*) after the initial inward current response evoked by 5-HT (45,46,51). This first inward current was tested for stability in 5-HT_{3A}Rs and all engineered constructs, except in 5-HT_{3A}-I409C/R410C and 5-HT_{3A}-QDA-I409C/R410C. Constructs containing Cys at positions I409 and R410 showed a current decrease with repeated agonist application (Fig. 3 *A*), and therefore, a stable response was not the requirement to proceed. All other constructs showed a stable current response before application of oxidizing reagent. After the 2-min exposure to Cu:Phe, the oocytes were washed for 6 min with OR-2 before another agonist-induced current was recorded (Fig. 4 *A*, second inward current) and tested for stability. Lastly, we investigated the effect of applying 10 mM DTT (Fig. 4 *A*; Fig. S3 *A*), a reducing agent capable of converting protein disulfides to sulfhydryls via thiol-disulfide exchange reaction, or 1 mM EGTA (Fig. 4 *B*; Fig. S3 *B*), a copper chelating agent (52). DTT or EGTA was applied to the same oocyte after Cu:Phe exposure for 2 min, followed by a 6-min OR-2 wash before another 5-HT application (final inward current, DTT: Fig. 4 *A*, EGTA: Fig. 4 *B*).

Overall, 5-HT-induced inward currents of 5-HT_{3A}-wt and 5-HT_{3A}-QDA receptors were unaffected by Cu:Phe, DTT, and EGTA (Fig. 4). The current amplitudes of 5-HT_{3A}-L402C/L403C showed no change after Cu:Phe or EGTA but increased by ~14% after exposure to DTT (Fig. 4 *C*; Fig. S3). The same Cys pair in the 5-HT_{3A}-QDA background, 5-HT_{3A}-QDA-L402C/L403C, showed reduced current amplitudes after Cu:Phe (71.7 $\pm$ 11.6% of initial, $n = 12$) as compared with the initial current, which could be recovered by either DTT or EGTA (Fig. 4 *C*; Fig. S3). Overall, Cu:Phe had the most pronounced effect on 5-HT_{3A}-I409C/R410C and 5-HT_{3A}-QDA-I409C/R410C, decreasing their inward current amplitudes to ~61 and ~29% of the initial inward current, respectively (Fig. 4), an effect not observed in the single-Cys construct, 5-HT_{3A}-I409C (Fig. S2). In the case of 5-HT_{3A}-I409C/R410C, the current responses after Cu:Phe were not stable, and the amplitudes were further attenuated to ~39% of the original current with repeated agonist application (Fig. 4, *middle panel*, third inward current evoked by 5-HT in sample traces). This

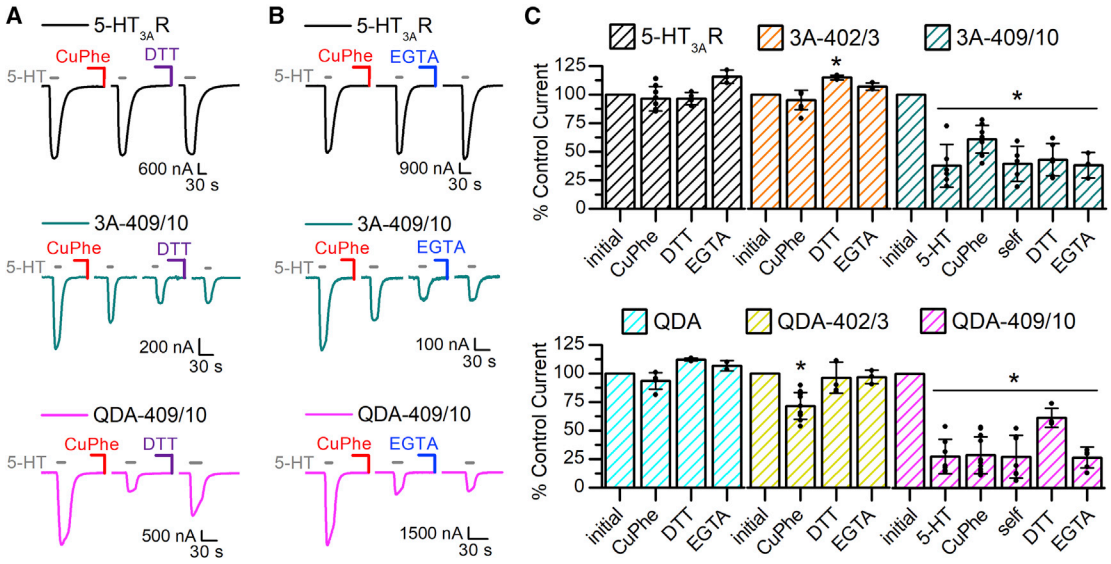

FIGURE 4 Effect of oxidizing (Cu:Phe), reducing (DTT), and chelating (EGTA) agents on 5-HT_{3A}Rs-wt and I409C/R410C Cys pairs. (*A*) Sample traces of 5-HT_{3A}-wt (*black*), 5-HT_{3A}-I409C/R410C (*green*), and QDA-I409C/R410C (*magenta*) are shown. The inward currents were evoked with 3 μM 5-HT. The initial inward current represents the reference current amplitude (100% of current). After the 5-HT application(s), the oocytes were exposed to 2 min of Cu:Phe (100:200 μM) and then a 6-min wash with OR-2 (not pictured) before another application of 5-HT (second inward current depicted). 5-HT was applied until a stable current response was achieved (stable response to 5-HT is the inward current before DTT, labeled "self" in (*C*) for I409C/R410C mutants). Lastly, 10 mM DTT was applied to the oocytes for 2 min, followed by a 6-min OR-2 wash (not pictured) and 5-HT (last inward current pictured). (*B*) Sample traces of 5-HT_{3A}-wt (*black*), 5-HT_{3A}-I409C/R410C (*green*), and QDA-I409C/R410C (*magenta*) are shown with the same experimental setup as in (*A*), but during the last step, 1 mM EGTA was applied instead of DTT. (*C*) Quantitative representation of current amplitudes, including Fig. 3 *C*, 5-HT and Fig. S3. The initial inward current represents 100% of the current response. Data are shown as mean ± SD. Individual data points are shown as circles overlaid on top of the bar graph ($n \geq 3$). Statistical significance was determined with one-way ANOVA, Dunnett's multiple comparisons test between the initial inward current and each set of conditions ($*p \leq 0.01$).

reduction in current response could not be recovered for 5-HT_{3A}-I409C/R410C with either DTT or EGTA application and could be partially recovered with DTT (61.6 ± 8.32% of initial current), but not EGTA, for 5-HT_{3A}-QDA-I409C/R410C.

DISCUSSION

In our study, we investigated the effect of constraining the cytosolic end of the MA-helices of 5-HT_{3A}Rs by using disulfide bond formation between engineered cysteines. Disulfide trapping is a powerful tool to analyze backbone and domain motions in proteins of unknown and known high-resolution structure, with the advantage that these experiments can be carried out in the native environment of the protein (42,49), including within the membrane. We engineered double-Cys pairs within the MA-helix of 5-HT_{3A} subunits with the goal of using intersubunit disulfide bonds between subunits to clamp the MA-helices in a constrained conformation to gain insight into the importance of the movement of the lower end of the MA-helices during gating. The Cys substitutions were introduced two and four helical turns below the lowest arginine (R416 or $-4'$, Fig. 1) located in the lateral portals, the part of the MA-helix that so far has been orphaned by functional studies. The same Cys pairs were introduced into the 5-HT_{3A}-QDA background that yields receptors with a ~33-fold increased conductance (25).

SDS-PAGE separation of crude membrane fractions followed by immunoblotting indicated that the MA-helices are cross-linked for both Cys pairs after treatment with agonist or oxidizing agent, manifested as bands representing dimers and higher-order oligomers (Fig. 2 *A*; (53)). Oligomer bands were only observed for the Cys pairs and not for 5-HT_{3A}-wt, 5-HT_{3A}-QDA, or single-Cys construct receptors (Fig. S2) and could be completely reduced to monomers in the presence of a reducing agent under denaturing conditions, ascertaining that these bands were indeed the result of disulfide bonds.

Functionally, for the double-Cys pairs at I409C-R410C, we observed agonist-induced decreases in current amplitude with either repeated or prolonged applications of 5-HT until a steady state was reached (Figs. 3 and 4). A more oxidizing environment mediated by the catalyst Cu:Phe also led to agonist-induced current amplitude reductions (Fig. 4), which were not stable or complete for this Cys pair in the 5-HT_{3A}-wt background. Agonist application reduced the current further for 5-HT_{3A}-I409C/R410C, but current reductions could not be recovered with either reducing or chelating agents. For 5-HT_{3A}-QDA-I409C/R410C, on the other hand, current reduction was partially reversed with DTT, but not the chelating agent EGTA, indicating that

the reduction in current is caused by disulfide bond formation and not heavy metal binding. Divalent cations such as Cu^{2+} have been shown to modulate 5-HT_3 receptor responses by interacting with the extracellular surface of the receptor (54). Chelating the extracellular copper ions can reverse this heavy metal binding effect, which leads to the recovery of agonist-induced current. Because both agonist application and an oxidizing agent lead to current reduction for the double-Cys pairs at I409C-R410C, we infer that the resultant chemical state is comparable, in that both treatments yield cross-linked intersubunit cystines.

The other Cys pairs at L402C-L403C only showed a small change in current response after agonist and oxidizing agent application. For 5-HT_{3A}-QDA-L402C/L403C, oxidizing reagent-induced current reduction and reductant- and EGTA-induced reversal were observed (Fig. 4 *C*; Fig. S3, *yellow*). The 5-HT_{3A}-L402C/L403C Cys pair only had a small current increase after DTT (Fig. 4 *C*).

Disulfide bond formation of cysteine side chains depends on the presence of an oxidizing environment as well as the sulfhydryl collision frequency, which is influenced by their separation distance, their orientation in the protein, and the backbone mobility in the region (55). Cross-linking in the absence of an oxidizing catalyst, as observed upon agonist administration for the Cys pairs at I409C-R410C, indicates a relatively high propensity for disulfide bond formation. The reaction mechanism does not differ fundamentally from cross-linking in more oxidizing environments created by Cu:Phe (55,56). In the case of I409C-R410C, agonist application(s) achieved a large and stable current reduction, suggesting that serotonin induces a motion in the receptor that promotes disulfide bond formation between these positions (57). In the presence of 5-HT, the channels undergo transitions between open, desensitized, and closed states. We cannot, with certainty, distinguish in which state agonist-induced disulfide bond formation occurs because of the millisecond timescale of transitioning (45,55).

The disulfide bond formation initiated by agonist application yields two subsets of information. Firstly, disulfide bonds have well-defined distance and angular constraints, which indicates close proximity for the two Cys when a cystine forms (42). Secondly, disulfide bond formation at I409-R410 puts structural constraints on the mechanism of conformational changes, giving insights into the relationship between structural changes and function (58). There are several factors that could mediate the reduction in current upon cross-linking, including a decrease in single-channel conductance (especially for the 5-HT_{3A}-QDA background), a change in open probability, locking the channels in a nonconducting conformation, and altered kinetics. Based on these data, we cannot distinguish between these possibilities.

SDS-PAGE separation and Western blot after treatments that favor cross-linking revealed that most of the cross-linked Cys pairs run as dimers as opposed to higher oligomers (Fig. 2 *B*). We infer that when two adjacent subunits are cross-linked by the formation of one disulfide bond within the pentamer, this disulfide bond also constrains the concerted movement of the other subunits, affecting the orientation and backbone mobility of the MA-helices.

Agonist-induced current reduction was absent for the Cys pairs at L402C-L403C (Fig. 3 *A*). A minimal current reduction after Cu:Phe application that was recovered after either DTT or EGTA incubation was observed, pointing toward a small inhibitory effect by heavy metal binding (Fig. 4 *C*) because both DTT and EGTA can act as metal chelators. Our results indicate that the cross-linking observed for L402C-L403C using SDS-PAGE separation and immunoblotting is largely functionally silent in macroscopic currents, which could indicate their proximity to each other in the equilibrium structure (49), and that conformational flexibility at the vertical end of the pore is not required for ion conduction.

A characteristic specific to the A subunit of 5-HT_3Rs is that the MA-helices are lined with positively and negatively charged residues that interact to form inter- and intrasubunit salt bridges (37,38). Another notable salt bridge is located between the MA-helix and the L1-loop; D312 at the center of L1 is straddled by the 0′ and 4′ arginine residues (mouse R420 and R424, human R436 and R440) from the MA-helix of the adjacent subunit. Amino acid substitutions introduced in the proximity of the five lateral portals, such as the QDA substitution, lead to the breakage of these salt bridges, which enhances flexibility of the MA-bundle, increases single-channel conductance, and disrupts pentamerization of the ICD (25,37,38). Based on these observations, we hypothesize that partial release of intersubunit salt bridges in the 5-HT_{3A}-QDA background yields a more open and unclamped or flexible arrangement of the ICD, in particular the MA-helices. This could explain our experimental differences observed between the 5-HT_{3A}-wt and 5-HT_{3A}-QDA backgrounds. The 5-HT_{3A}-QDA-I409C/R410C Cys pair has a ∼10% larger current reduction after the restriction of its increased MA-mobility after 5-HT application as compared with the same Cys pair in the 5-HT_{3A}-wt background, whereas the current reduction is significantly different by ∼30% directly after Cu:Phe application between the two backgrounds (unpaired *t*-test, $t(19) = 5.21$, $p = 4.96 \times 10^{-5}$). The overall quantification of band intensities for each construct in each condition revealed that the Cys pairs in the 5-HT_{3A}-QDA background show higher percentages for dimers and some higher oligomeric states as compared to the 5-HT_{3A}-wt background (Fig. 2 *B*).

5-HT_{3A}-QDA-I409C/R410C could also be partially recovered with DTT (Fig. 4 *C*). Based on the mechanism of the involved redox chemistry, reduction with DTT involves a disulfide exchange reaction, necessitating access of the DTT molecule in close apposition to the disulfide bond to be reduced. Therefore, the inability to reverse oxidation with DTT may be due to the reduced accessibility

of the less mobile and rigid MA-bundles in the 5-HT_{3A}-wt background (37) and an increased mobility mediated by the 5-HT_{3A}-QDA substitutions.

Overall, we conclude that disulfide bonds form for both double-cysteine pairs based on oligomers observed after immunoblotting and our functional data. We infer that conformational changes associated with gating are more pronounced for the upper I409C-R410C pair that sits three helical turns below the frame of the lateral windows and on the upper end of the hydrophobic plug. The area below this plug, where the helices converge, seems to be involved in smaller motions, whereas the ICD above twists around the central pore of the receptor.

These findings can be compared to the mechanics of an umbrella, in which the MA-helices represent the rods of the umbrella. In the inverted umbrella, the ferrule or top notch corresponds to the cytosolic end of the MA-helices. Low on the converging rods or MA-helices, we find L402C-L403C, whereas I409C-R410C is positioned toward the top of the rods (Fig. 5). When the umbrella is closed (i.e., the receptor is in a non-conducting state) the rods are aligned with the shaft (ion pore) in a vertical line, and both the lower (L402C-L403C) and upper portion (I409C-R410C) of the rods are in close proximity to corresponding adjacent rod positions. When the umbrella opens, the upper rod positions (I409C-R410C) move outward to allow for the canopy to open, whereas the lower positions closer to the notch (L402C-L403C) undergo smaller movements at the end of the shaft.

Structures indicate a clockwise rotational movement of the TMD between closed and open states (4). The TMD is structurally linked to the ICD by the continuation of the M4 transmembrane segment into the MA-helix. This twisting movement of the MA-helices could break the salt bridge network, including D312, that holds the L1-loop in place, resulting in the L1-loop moving outward, which in turn allows translation of the MX-helix toward the membrane inner leaflet (Fig. S1).

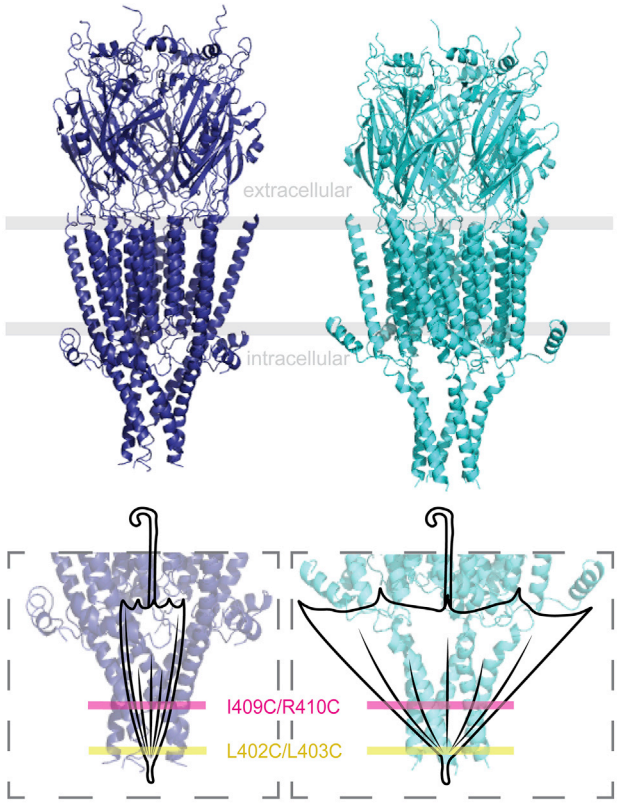

FIGURE 5 Umbrella analogy of MA-helix mobility. (*top*) Cartoon representation of 5-HT_{3A}Rs in different conducting states (*blue*, PDB: 6BE1; *cyan*, PDB: 6DG8) is shown with approximate locations inside the membrane (*gray lines*). (*bottom*) Zoomed-in view of the ICD for the umbrella analogy is given: the MA-helices move in a comparable fashion between closed and open states as do umbrella rods between closed and open states. The L402C-L403C (*yellow*) Cys pair is located closer to the top notch, where the rods of the umbrella converge, and I409C-R410C (*magenta*) further away from the ferrule. When the umbrella is closed (the receptor is in a non-conducting state; *blue* (PDB: 6BE1)), the rods are aligned with the shaft of the umbrella. The rods are stretched away when the canopy opens (receptor in a conducting state; *cyan* (PDB: 6DG8)). Note that the distance changes between rod positions closer to the ferrule or top notch are smaller and increase with increasing distance to the ferrule.

CONCLUSIONS

Our results investigate the importance of the mobility of the cytosolic end of the MA-helices by using a disulfide chemistry approach. Intersubunit cross-linking through agonist activation or oxidation three helical turns below the lateral portals leads to smaller macroscopic currents. This indicates that the mobility or flexibility of the MA-helices below the lateral portals is required to open the cytosolic ion pathway. In contrast, disulfide bond formation at the cytosolic end of the MA-helices, where the helices converge, is functionally silent in macroscopic currents. The absence of a functional effect of this disulfide cross-linking further supports that ions do not exit the cytosolic vestibule along the long channel axis but instead through five lateral portals that open through concerted conformational changes involving MA-helices, L1-loops, and by extension, also MX-helices. The mobility of the ICD we infer here as being required for conformational changes of the channel to open is also consistent with recent observations gleaned from structural studies of cation-conducting pLGICs obtained with single-particle cryo-EM. Cryo-EM imaging in the presence of the agonist yielded heterogeneity in the 5-HT_{3A}R membrane domain, and further three-dimensional classification yielded two subsets of particles with differing conformations (Protein Data Bank, PDB: 6HIN, 6HIO) (7). Of note, for one of these conformations, the ICD could not be resolved, which led to it being described as "a very dynamic ICD, beyond the intrinsically disordered region" (PDB: 6HIN). At the same time, this conformation displays a wider transmembrane pore diameter consistent with wetting and ion conduction, whereas the conformation with resolved ICD

is non-conducting (PDB: 6HIO). In a study of muscle-type nAChRs, the ICD could be resolved when an additional classification step sorted particles based on whether the ECD was ordered, thus focusing on a subset of receptor-like particles (59). Therefore, our functional and cross-linking data are supported by very recent structural data of cation-conducting pLGICs. Further studies are needed to investigate the concerted mechanism and movements and may lead to the identification of a future therapeutic target because the MA-helices can affect channel function.

SUPPORTING MATERIAL

Supporting Material can be found online at https://doi.org/10.1016/j.bpj.2020.10.029.

AUTHOR CONTRIBUTIONS

M.J. and A.G.S. designed research. A.G.S. performed experiments. A.G.S. and M.J. analyzed data. A.G.S. and M.J. wrote the article.

ACKNOWLEDGMENTS

We thank the TTUHSC Core Facilities; some of the images and/or data were generated in the Image Analysis Core Facility and Molecular Biology Core Facility supported by TTUHSC.

Research reported in this publication was supported by the National Institute of Neurological Disorders and Stroke of the National Institutes of Health under award number R01/R56NS077114 (to M.J.).

REFERENCES

1. Thompson, A. J., H. A. Lester, and S. C. Lummis. 2010. The structural basis of function in Cys-loop receptors. *Q. Rev. Biophys.* 43:449–499.
2. Thompson, A. J., and S. C. Lummis. 2013. Discriminating between 5-HT_3A and 5-HT_3AB receptors. *Br. J. Pharmacol.* 169:736–747.
3. Baptista-Hon, D. T., T. Z. Deeb, …, T. G. Hales. 2013. The minimum M3-M4 loop length of neurotransmitter-activated pentameric receptors is critical for the structural integrity of cytoplasmic portals. *J. Biol. Chem.* 288:21558–21568.
4. Basak, S., Y. Gicheru, …, S. Chakrapani. 2018. Cryo-EM reveals two distinct serotonin-bound conformations of full-length 5-HT_{3A} receptor. *Nature.* 563:270–274.
5. Basak, S., Y. Gicheru, …, S. Chakrapani. 2018. Cryo-EM structure of 5-HT_{3A} receptor in its resting conformation. *Nat. Commun.* 9:514.
6. Hassaine, G., C. Deluz, …, H. Nury. 2014. X-ray structure of the mouse serotonin 5-HT3 receptor. *Nature.* 512:276–281.
7. Polovinkin, L., G. Hassaine, …, H. Nury. 2018. Conformational transitions of the serotonin 5-HT_3 receptor. *Nature.* 563:275–279.
8. Gharpure, A., J. Teng, …, R. E. Hibbs. 2019. Agonist selectivity and ion permeation in the α3β4 ganglionic nicotinic receptor. *Neuron.* 104:501–511.e6.
9. Morales-Perez, C. L., C. M. Noviello, and R. E. Hibbs. 2016. X-ray structure of the human α4β2 nicotinic receptor. *Nature.* 538:411–415.
10. Unwin, N. 2005. Refined structure of the nicotinic acetylcholine receptor at 4A resolution. *J. Mol. Biol.* 346:967–989.
11. Walsh, R. M., Jr., S. H. Roh, …, R. E. Hibbs. 2018. Structural principles of distinct assemblies of the human α4β2 nicotinic receptor. *Nature.* 557:261–265.
12. Miyazawa, A., Y. Fujiyoshi, …, N. Unwin. 1999. Nicotinic acetylcholine receptor at 4.6 A resolution: transverse tunnels in the channel wall. *J. Mol. Biol.* 288:765–786.
13. Halevi, S., L. Yassin, …, M. Treinin. 2003. Conservation within the RIC-3 gene family. Effectors of mammalian nicotinic acetylcholine receptor expression. *J. Biol. Chem.* 278:34411–34417.
14. Lansdell, S. J., V. J. Gee, …, N. S. Millar. 2005. RIC-3 enhances functional expression of multiple nicotinic acetylcholine receptor subtypes in mammalian cells. *Mol. Pharmacol.* 68:1431–1438.
15. Williams, M. E., B. Burton, …, J. Aiyar. 2005. Ric-3 promotes functional expression of the nicotinic acetylcholine receptor alpha7 subunit in mammalian cells. *J. Biol. Chem.* 280:1257–1263.
16. Cheng, A., N. A. McDonald, and C. N. Connolly. 2005. Cell surface expression of 5-hydroxytryptamine type 3 receptors is promoted by RIC-3. *J. Biol. Chem.* 280:22502–22507.
17. Lansdell, S. J., T. Collins, …, N. S. Millar. 2008. Host-cell specific effects of the nicotinic acetylcholine receptor chaperone RIC-3 revealed by a comparison of human and Drosophila RIC-3 homologues. *J. Neurochem.* 105:1573–1581.
18. Pandhare, A., P. N. Grozdanov, and M. Jansen. 2016. Pentameric quaternary structure of the intracellular domain of serotonin type 3A receptors. *Sci. Rep.* 6:23921.
19. Nishtala, S. N., N. Mnatsakanyan, …, M. Jansen. 2016. Direct interaction of the resistance to inhibitors of cholinesterase type 3 protein with the serotonin receptor type 3A intracellular domain. *J. Neurochem.* 137:528–538.
20. Mnatsakanyan, N., S. N. Nishtala, …, M. Jansen. 2015. Functional chimeras of GLIC obtained by adding the intracellular domain of anion- and cation-conducting Cys-loop receptors. *Biochemistry.* 54:2670–2682.
21. Goyal, R., A. A. Salahudeen, and M. Jansen. 2011. Engineering a prokaryotic Cys-loop receptor with a third functional domain. *J. Biol. Chem.* 286:34635–34642.
22. Jansen, M., M. Bali, and M. H. Akabas. 2008. Modular design of Cys-loop ligand-gated ion channels: functional 5-HT3 and GABA rho1 receptors lacking the large cytoplasmic M3M4 loop. *J. Gen. Physiol.* 131:137–146.
23. Pirayesh, E., A. G. Stuebler, …, M. Jansen. 2020. Delineating the site of interaction of the 5-HT_{3A} receptor with the chaperone protein RIC-3. *Biophys. J.* 118:934–943.
24. Livesey, M. R., M. A. Cooper, …, J. A. Peters. 2008. Structural determinants of Ca2+ permeability and conduction in the human 5-hydroxytryptamine type 3A receptor. *J. Biol. Chem.* 283:19301–19313.
25. Kelley, S. P., J. I. Dunlop, …, J. A. Peters. 2003. A cytoplasmic region determines single-channel conductance in 5-HT3 receptors. *Nature.* 424:321–324.
26. Miyazawa, A., Y. Fujiyoshi, and N. Unwin. 2003. Structure and gating mechanism of the acetylcholine receptor pore. *Nature.* 423:949–955.
27. Carland, J. E., M. A. Cooper, …, J. J. Lambert. 2013. Mutagenic analysis of the intracellular portals of the human 5-HT3A receptor. *J. Biol. Chem.* 288:31592–31601.
28. Deeb, T. Z., J. E. Carland, …, T. G. Hales. 2007. Dynamic modification of a mutant cytoplasmic cysteine residue modulates the conductance of the human 5-HT3A receptor. *J. Biol. Chem.* 282:6172–6182.
29. Hales, T. G., J. I. Dunlop, …, J. A. Peters. 2006. Common determinants of single channel conductance within the large cytoplasmic loop of 5-hydroxytryptamine type 3 and alpha4beta2 nicotinic acetylcholine receptors. *J. Biol. Chem.* 281:8062–8071.
30. Peters, J. A., J. E. Carland, …, J. J. Lambert. 2006. Novel structural determinants of single-channel conductance in nicotinic acetylcholine and 5-hydroxytryptamine type-3 receptors. *Biochem. Soc. Trans.* 34:882–886.
31. Du, J., W. Lü, …, E. Gouaux. 2015. Glycine receptor mechanism elucidated by electron cryo-microscopy. *Nature.* 526:224–229.

32. Sauguet, L., A. Shahsavar, …, M. Delarue. 2014. Crystal structures of a pentameric ligand-gated ion channel provide a mechanism for activation. *Proc. Natl. Acad. Sci. USA.* 111:966–971.

33. Bocquet, N., H. Nury, …, P. J. Corringer. 2009. X-ray structure of a pentameric ligand-gated ion channel in an apparently open conformation. *Nature.* 457:111–114.

34. Bocquet, N., L. Prado de Carvalho, …, P. J. Corringer. 2007. A prokaryotic proton-gated ion channel from the nicotinic acetylcholine receptor family. *Nature.* 445:116–119.

35. Hilf, R. J., and R. Dutzler. 2009. Structure of a potentially open state of a proton-activated pentameric ligand-gated ion channel. *Nature.* 457:115–118.

36. Ilegems, E., H. Pick, …, H. Vogel. 2005. Ligand binding transmits conformational changes across the membrane-spanning region to the intracellular side of the 5-HT3 serotonin receptor. *ChemBioChem.* 6:2180–2185.

37. Kozuska, J. L., I. M. Paulsen, …, S. M. Dunn. 2014. Impact of intracellular domain flexibility upon properties of activated human 5-HT3 receptors. *Br. J. Pharmacol.* 171:1617–1628.

38. Pandhare, A., E. Pirayesh, …, M. Jansen. 2019. Triple arginines as molecular determinants for pentameric assembly of the intracellular domain of 5-HT_{3A} receptors. *J. Gen. Physiol.* 151:1135–1145.

39. Reeves, D. C., E. N. Goren, …, S. C. Lummis. 2001. Structural and electrostatic properties of the 5-HT3 receptor pore revealed by substituted cysteine accessibility mutagenesis. *J. Biol. Chem.* 276:42035–42042.

40. Stuebler, A. G., and M. Jansen. 2020. Bupropion inhibits serotonin type 3AB heteromeric channels at clinically relevant concentrations. *Mol. Pharmacol.* 97:171–179, Published online December 23, 2019.

41. Pandhare, A., A. S. Pappu, …, M. Jansen. 2017. The antidepressant bupropion is a negative allosteric modulator of serotonin type 3A receptors. *Neuropharmacology.* 113:89–99.

42. Careaga, C. L., and J. J. Falke. 1992. Thermal motions of surface alpha-helices in the D-galactose chemosensory receptor. Detection by disulfide trapping. *J. Mol. Biol.* 226:1219–1235.

43. Schmidt, B., L. Ho, and P. J. Hogg. 2006. Allosteric disulfide bonds. *Biochemistry.* 45:7429–7433.

44. Horenstein, J., D. A. Wagner, …, M. H. Akabas. 2001. Protein mobility and GABA-induced conformational changes in GABA(A) receptor pore-lining M2 segment. *Nat. Neurosci.* 4:477–485.

45. Jansen, M., and M. H. Akabas. 2006. State-dependent cross-linking of the M2 and M3 segments: functional basis for the alignment of GABAA and acetylcholine receptor M3 segments. *J. Neurosci.* 26:4492–4499.

46. Mnatsakanyan, N., and M. Jansen. 2013. Experimental determination of the vertical alignment between the second and third transmembrane segments of muscle nicotinic acetylcholine receptors. *J. Neurochem.* 125:843–854.

47. Reeves, D. C., M. Jansen, …, M. H. Akabas. 2005. A role for the beta 1-beta 2 loop in the gating of 5-HT3 receptors. *J. Neurosci.* 25:9358–9366.

48. Amin, D. N., B. L. Taylor, and M. S. Johnson. 2006. Topology and boundaries of the aerotaxis receptor Aer in the membrane of *Escherichia coli*. *J. Bacteriol.* 188:894–901.

49. Bass, R. B., S. L. Butler, …, J. J. Falke. 2007. Use of site-directed cysteine and disulfide chemistry to probe protein structure and dynamics: applications to soluble and transmembrane receptors of bacterial chemotaxis. *Methods Enzymol.* 423:25–51.

50. Kobashi, K. 1968. Catalytic oxidation of sulfhydryl groups by o-phenanthroline copper complex. *Biochim. Biophys. Acta.* 158:239–245.

51. Wiltfong, R. E., and M. Jansen. 2009. Probing protein packing surrounding the residues in and flanking the nicotinic acetylcholine receptor M2M3 loop. *J. Neurosci.* 29:1626–1635.

52. Fisher, A. E., T. A. Hague, …, D. P. Naughton. 2004. Catalytic superoxide scavenging by metal complexes of the calcium chelator EGTA and contrast agent EHPG. *Biochem. Biophys. Res. Commun.* 323:163–167.

53. Bali, M., M. Jansen, and M. H. Akabas. 2009. GABA-induced intersubunit conformational movement in the GABAA receptor alpha 1M1-beta 2M3 transmembrane subunit interface: experimental basis for homology modeling of an intravenous anesthetic binding site. *J. Neurosci.* 29:3083–3092.

54. Lovinger, D. M. 1991. Inhibition of 5-HT3 receptor-mediated ion current by divalent metal cations in NCB-20 neuroblastoma cells. *J. Neurophysiol.* 66:1329–1337.

55. Bera, A. K., and M. H. Akabas. 2005. Spontaneous thermal motion of the GABA(A) receptor M2 channel-lining segments. *J. Biol. Chem.* 280:35506–35512.

56. Borghese, C. M., J. A. Hicks, …, R. A. Harris. 2014. GABA(A) receptor transmembrane amino acids are critical for alcohol action: disulfide cross-linking and alkyl methanethiosulfonate labeling reveal relative location of binding sites. *J. Neurochem.* 128:363–375.

57. Chrisman, P. A., J. I. Podair, …, M. M. Levandoski. 2014. Intra-subunit flexibility underlies activation and allosteric modulation of neuronal nicotinic acetylcholine receptors. *Neuropharmacology.* 79:420–431.

58. de la Peña, P., C. Alonso-Ron, …, F. Barros. 2011. Demonstration of physical proximity between the N terminus and the S4-S5 linker of the human ether-a-go-go-related gene (hERG) potassium channel. *J. Biol. Chem.* 286:19065–19075.

59. Rahman, M. M., J. Teng, …, R. E. Hibbs. 2020. Structure of the native muscle-type nicotinic receptor and inhibition by snake venom toxins. *Neuron.* 106:952–962.e5.